A Distributed Power Control of Series-Connected Module-Integrated Inverters for PV Grid-Tied Applications

Li Zhang, *Member, IEEE*, Kai Sun, *Senior Member, IEEE*, Yun Wei Li, *Senior Member, IEEE*, Xiaonan Lu, *Member, IEEE*, and Jinquan Zhao, *Member, IEEE*

***Abstract*—To enhance the redundancy and reliability for a distributed generation system, a grid-tied photovoltaic (PV) generation system based on series-connected module-integrated inverters (SC-MIIs) is presented in this paper. In the grid-tied SC-MII system, each PV panel is interfaced with an MII with independent maximum power point tracking to harvest maximum solar energy. The outputs of MIIs are at ac line frequency and are connected in series to fulfill the voltage requirement in the utility grid. Since the high step-up power conversion stage in the conventional microinverter is avoided, the grid-tied SC-MII system is easier to implement and features high efficiency. Meanwhile, a distributed control strategy for SC-MIIs is proposed, in which the active power sharing among the MIIs depends on the individual maximum power available from PV panels, while the reactive power of the system can be regulated by any of the MIIs according to the utility grid command. Simulation and experimental results verify the feasibility and effectiveness of the proposed system and its corresponding control strategy.**

***Index Terms*—Grid-tied inverters, inverters, module-integrated inverters (MIIs), photovoltaic (PV) generation, series connected.**

I. Introduction

DISTRIBUTED photovoltaic (PV) generation has been extensively developed in both commercial and residential systems over the past decades. Due to the low energy conversion efficiency of PV panels, current research still focuses on maximizing the energy harvested from PV panels and improving the conversion efficiency of the power conditioning stage [1]–[5]. However, the mismatches induced by manufacturing tolerances, partial shading, dirt on the surface of PV panels, thermal gradients, or aging result in losses in energy captured by a PV energy conversion system. Furthermore, mismatched PV modules or systems exhibit a nonconvex attribute of output power with respect to output voltage, which hinders the operation of maximum power point (MPP) tracking algorithm and results in the need to operate PV grid-tied inverters over a wider range of MPP voltages [6]. Distributed maximum power point tracking (DMPPT) allows one to overcome the drawbacks associated with mismatching phenomena.

Many state-of-the-art architectures of a PV grid-tied system based on DMPPT techniques have been proposed, including the ac-module structure, the dc-module structure, the distributed differential power processing (DPP) structure, and the series-connected H-bridge structure [7], [8], as shown in Fig. 1. The ac module, as shown in Fig. 1(a), is also called the module-integrated converter (MIC). The MIC can be used as a plug-in device by individual users without professional knowledge. However, when compared with the string inverters, MICs have lower efficiencies and higher cost per watt [9]–[11]. In most of the existing MIC topologies, a high-frequency transformer is used to boost the low PV voltage so that it matches the utility grid voltage. A high switching frequency is necessary to achieve a compact inverter size. As a result, both the switching losses of the MIC devices and the transformer losses are the dominant limitations for improving the efficiency. The dc module structure integrates each PV panel with a dc/dc converter. The output ports of dc/dc converters are connected in series and the resulting string feeds in a centralized inverter [12], [13], as shown in Fig. 1(b). The voltage gain requirement in dc/dc converter topologies is reduced, and the dc-module structure leads to higher energy extraction with respect to the centralized MPPT. However, due to the limited voltage and current ratings of the adopted power devices and nonoptimal string voltage, extracting the maximum available power from each PV panel is not always achievable in mismatched conditions [14]–[18]. To further improve the performance, the DMPPT function carried out in the dc/dc converters should be in accordance with

Manuscript received May 27, 2017; revised September 21, 2017; accepted October 30, 2017. Date of publication November 1, 2017; date of current version June 22, 2018. This work was supported in part by the National Natural Science Foundation of China under Grant 51307096, in part by the 13th Six Talent Peaks Project in Jiangsu Province under Grant XNY-008, in part by the Beijing Science and Technology Plan under Grant Z161100002616039, in part by the Suzhou-Tsinghua Innovation Leading Action Program under Grant 2016SZ0301, in part by the Fundamental Research Funds for the Central Universities of China under Grant 2015B02314, in part by a Project Funded by the Priority Academic Program Development of Jiangsu Higher Education Institutions, and in part by the Tsinghua University-University of Alberta Joint Research Fund. Recommended for publication by Associate Editor M. Vitelli. *(Corresponding author: Kai Sun.)*

L. Zhang and J. Zhao are with the College of Energy and Electrical Engineering, Hohai University, Nanjing 211100, China (e-mail: zhanglinuaa@hhu.edu.cn; zhaojinquan@hhu.edu.cn).

K. Sun is with the State Key Laboratory of Power Systems, Department of Electrical Engineering, Tsinghua University, Beijing 100084, China (e-mail: sun-kai@mail.tsinghua.edu.cn).

Y. W. Li is with the Department of Electrical and Computer Engineering, University of Alberta, Edmonton, AB T6G 2V4, Canada (e-mail: yunwei.li@ualberta.ca).

X. Lu is with the Energy Systems Division, Argonne National Laboratory, Lemont, IL 60439 USA (e-mail: xiaonan.lu@ieee.org).

Color versions of one or more of the figures in this paper are available online at http://ieeexplore.ieee.org.

Digital Object Identifier 10.1109/TPEL.2017.2769487

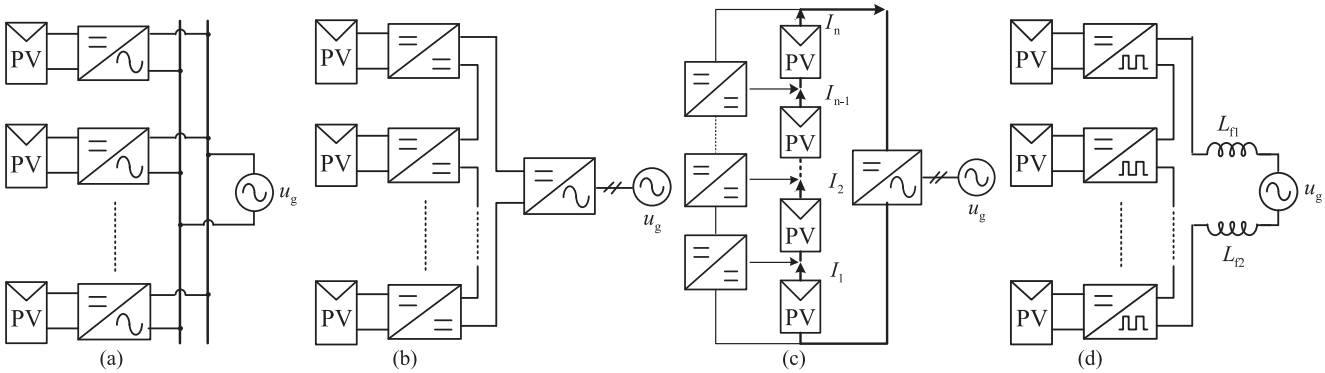

Fig. 1. Four architectures of a PV grid-tied system. (a) AC module. (b) DC module. (c) DPP. (d) Series-connected H-bridge.

the centralized MPPT function carried out in the centralized inverter [16]. Therefore, the number of dc modules in a string should be careful designed. On the other hand, the maximum power capacity of the dc module structure depends on the power rating of the centralized inverter, which limits the scalability of the system. Meanwhile, the power stage of the inverter lacks sufficient redundancy as well. As opposed to the dc module structure, the DPP structure directly bypasses most of the power and handles only the local mismatch to achieve local MPP with low-power converters [19]–[21], as shown in Fig. 1(c). Therefore, the lower power rating of DPP converters offers a potential cost reduction and reliability enhancement as well as higher efficiency. However, a centralized inverter is still required in the DPP structure. The series-connected H-bridge structure also mandates a lower voltage gain requirement for each module, as shown in Fig. 1(d). This structure can also be called cascaded H-bridge converters in some industrial applications, such as motor drives and STATCOM, which are connected with symmetrical individual dc sources [22]–[25]. Therefore, this structure can achieve direct medium-voltage grid access without using bulky medium-voltage transformers. However, the series-connected H-bridge in PV systems is different. Particularly, the input voltage of each submodule is different in the series-connected H-bridge. As the same grid-tied current flows through the ac side of each module, the active power mismatch will result in a different ac output voltage of these modules [26]. The module with higher active power generation will carry a greater portion of the whole ac output voltage, which may cause overmodulation and degrade power quality. On the other hand, the series-connected H-bridge features a high equivalent output pulse width modulation (PWM) frequency [27]–[30]. Both the enhanced system efficiency and the reduced output filter size are achieved in this system. However, although the active power distribution among series-connected H-bridge modules is determined by the individual maximum power available from PV panels, a centralized controller is still indispensable to regulate the grid-tied current in the dc/ac stage. Therefore, the stage of the inverter is lack of redundancy as well.

Based on the above analysis, an advanced PV generation system should have characteristics such as high reliability, high efficiency, flexible controllability, and excellent scalability. A grid-tied PV generation system based on series-connected module-integrated inverters (SC-MIIs) was presented in [31]. The outputs of the MIIs are at ac line frequency and are connected in series to fulfill the voltage requirement in the utility grid. Since the high step-up power conversion in conventional microinverters is eliminated, the SC-MII structure has potential cost and efficiency advantages. Based on this structure, an autonomous control has been proposed in [32]. Each MII has a slow outer control loop for the input voltage and a fast inner control loop for the ac output power. However, only the steady-state operation of the systems was presented. The reactive power control of the system has not been presented, and nonunity power factor operation of this system has not been discussed as well.

A distributed control strategy for SC-MIIs is proposed in this paper, in which the active power sharing between MIIs depends on the individual maximum power available from PV panels without a centralized controller, while the reactive power of the system can be regulated through any individual MII. The rest of this paper is organized as follows: the structure of the grid-tied PV generation system based on SC-MIIs is presented in Section II, where it is compared with the ac-module system, the dc-module system, the DPP system, and the series-connected H-bridge system. The power flow analysis of the grid-tied SC-MII system is also presented. In Section III, a distributed control strategy for the grid-tied SC-MII system is proposed. In Section IV, a downscaled prototype of the proposed PV system with three MIIs is built in the laboratory. Experimental results from the prototype are presented to verify the validity of the proposed control strategy. Finally, Section V concludes this paper.

II. System Architecture and Power Flow Analysis

A. System Architecture

The grid-tied PV generation system based on SC-MIIs is shown in Fig. 2, where u_{o1} to u_{on} represent the output voltages of each MII. The voltage at point of common coupling (PCC), *i.e.*, u_{PCC}, is the sum of the voltage of each MII. u_g represents the utility grid voltage, and Z_{Line} represents the line impedance.

Similar to the series-connected H-bridge, each PV panel is interfaced with an MII in the grid-tied SC-MII system. The outputs of MIIs are connected in series to achieve high-voltage level. The independent MPPT is achieved to harvest as much

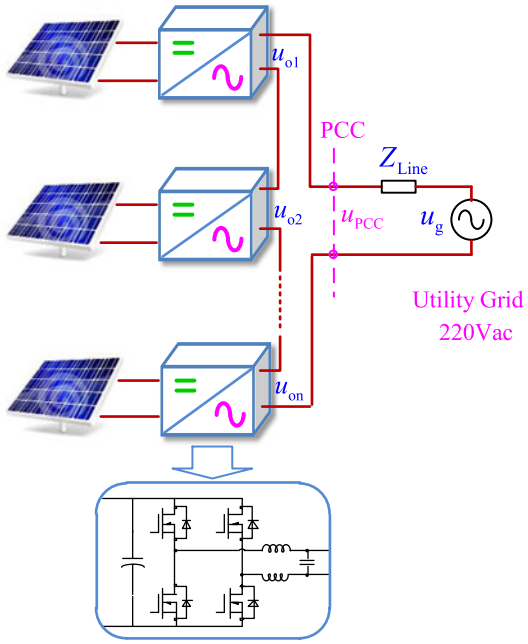

Fig. 2. Architecture of the grid-tied SC-MII system.

as solar energy in each MII. However, the outputs of MIIs are at ac line frequency in the grid-tied SC-MII system, while the outputs of the series-connected H-bridge are at PWM frequency. Therefore, each MII is an independent inverter with an output filter in the grid-tied SC-MII system, so the distributed control is easier to realize. In Fig. 2, each MII is implemented by using a single-phase full bridge inverter with the unipolar PWM. The total filter inductance of the SC-MII system structure is larger than that of the series-connected H-bridge. The total filter inductance of the SC-MII system structure can be calculated as

$$L_{f\_\mathrm{MII}} = \frac{n \cdot U_{\mathrm{PVmpp}}}{4 \cdot \Delta I_{Lf\max} \cdot f_s} \tag{1}$$

where U_{PVmpp} is the MPP voltage of each PV panel. $\Delta I_{Lf\max}$ is the maximum ripple current of inductors in each MII, and f_s is the switching frequency of each MII. n is not only defined as the number of SC-MIIs, but also defined as the number of submodules in the series-connected H-bridge.

The total filter inductance of the series-connected H-bridge can be written as

$$L_{f\_\mathrm{CMI}} = \frac{U_{\mathrm{PVmpp}}}{4 \cdot \Delta I_{Lf\max} \cdot f_{s\_\mathrm{eq}}} \tag{2}$$

where f_{s_eq} is the equivalent output PWM frequency. Due to the phase-shift carrier-based PWM control, the series-connected H-bridge generates $(2n + 1)$-level output voltage. The equivalent output PWM frequency (i.e., f_{s_eq}) is equal to $n \cdot f_s$. Therefore, with the same parameters, such as the number of series-connected modules, the switching frequency, the MPP voltage, and the maximum inductor ripple current, L_{f_MII} is larger than L_{f_CMI}.

The grid-tied SC-MII PV generation system has the following characteristics as well:

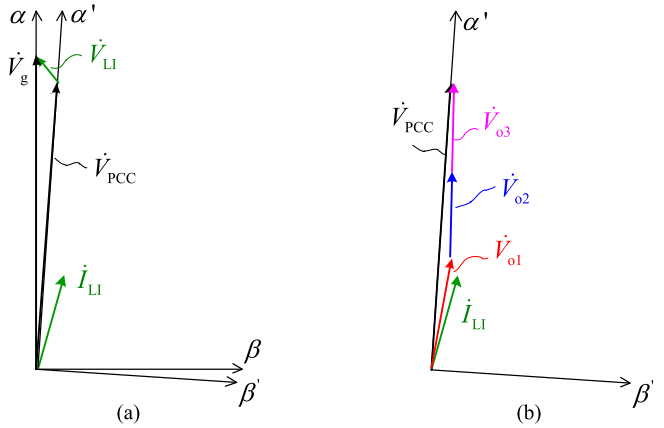

Fig. 3. Phasor diagrams showing the relation between the $\alpha\beta$ frame and the $\alpha'\beta'$ frame. (a) Relationship between grid-tied current, grid voltage, and PCC voltage of SC-MIIs, when grid-tied current lags grid voltage. (b) Voltage distribution of the SC-MIIs with reactive power control.

1) Compared with the ac module structure, the grid-tied SC-MII system reduces the voltage gain requirement for SC-MII topologies. Thus, the system efficiency can be improved.
2) Compared with the dc module structure and the DPP structure, the SC-MIIs are distributed and modularized instead of a centralized inverter. Therefore, the reliability of the grid-tied SC-MII system is higher than that of the dc module structure.
3) The power conditioning stage of the SC-MIIs can be single stage or two stage. Compared with the two-stage topology structure, the single-stage topology structure such as the H-bridge inverter can achieve higher system efficiency. However, the H-bridge inverter lacks the boost function, so that the inverter module must be designed with the lowest voltage of the wide-range PV input.

B. Power Flow Analysis

In the grid-tied SC-MII system, the same grid-tied current flows through the ac side of each MII. Therefore, the output voltage of each MII will determine the active and reactive power distribution. To clarify the power distribution, the series-connected system with three MIIs is taken as an example for analysis. The phasor diagram between the output voltage of each MII and the grid-tied current is depicted in Fig. 3, where $\dot{V}_g$ represents the utility grid voltage vector. $\dot{V}_{\mathrm{PCC}}$ represents the PCC voltage vector of SC-MIIs. $\dot{V}_{o1}$–$\dot{V}_{o3}$ represent output voltage vectors of MII #1–MII #3, respectively. $\dot{I}_{\mathrm{LI}}$ represents the grid-tied current vector. $\dot{V}_{\mathrm{LI}}$ represents the voltage vector of the line impedance.

From Fig. 3(a), it can be seen that the grid-tied current lagging the utility grid voltage is taken as an example for analysis. The α-axis is in phase with the utility grid voltage, and the β-axis lags the α-axis by 90°. Considering the line impedance, a new α'β' frame can be defined. In this frame, the α'-axis is in phase with the PCC voltage vector of SC-MIIs, and the β'-axis lags the α'-axis by 90°. The PCC voltage vector (i.e., $\dot{V}_{\mathrm{PCC}}$) should be synthesized by the output voltage vectors of three MIIs. If the reactive power control loop of each MII is disabled, the output

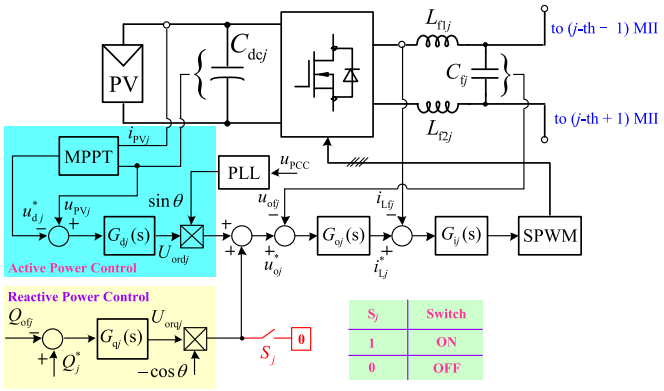

Fig. 4. Control scheme of MIIs.

voltage vector reference of each MII is aligned with the α'-axis following the phase-locked loop (PLL). Therefore, the power factor of the SC-MII system cannot be regulated. Furthermore, the phase of the grid-tied current cannot be controlled. As a result, the SC-MII system is unstable without the reactive power control. The grid-tied current lagging grid voltage is taken as an example for analysis. Assuming that the reactive power control loop of MII #1 is enabled, the voltage vector reference of MII #1 contains a positive β'-axis component generated by the reactive power control loop. As a result, the output voltage vector of MII #1 lags the PCC voltage vector, as shown in Fig. 3(b). Both the reactive power control loops of MII #2 and MII #3 are disabled. Thus, both the voltage vector references of MII #2 and MII #3 are still in phase with the PCC voltage vector, while the output voltage vectors of MII #2 and MII #3 lead the PCC voltage. It is obvious that if reactive power control loops of all the MIIs are enabled, the output voltage vectors of all the MIIs will lag the PCC voltage. Thus, the PCC voltage vector cannot be synthesized by output voltage vectors of three MIIs. On the other hand, since the same grid-tied current flows though the ac side of each MII, the reactive power of each MII is coupled. Therefore, only one MII is available to enable its reactive power control loop. The same analysis can be extended to the condition with the grid-tied current leading the utility grid voltage.

III. Control Strategy and Implementation Consideration

A. Control Scheme Analysis

Fig. 4 shows the control scheme of the *j*th single-stage MII.

The same control scheme can be applied to the other MIIs, where $u_{\mathrm{PV}j}$ and $i_{\mathrm{PV}j}$ represent the output voltage and current of the *j*th PV panel, respectively. u^*_{dj} is the output signal of the *j*th MPPT unit. u_{PCC} represents the PCC voltage. $\sin\theta$ is the output of the PLL, and it is in phase with the PCC voltage, u_{PCC}. $U_{\mathrm{ord}j}$ is the output of $G_{dj}(\mathrm{s})$, and $U_{\mathrm{orq}j}$ is the output of $G_{qj}(\mathrm{s})$. Q^*_j and $Q_{\mathrm{of}j}$ are defined as the reference and feedback of the reactive power of the *j*th MII, respectively. u^*_{oj} and u_{ofj} represent the reference and feedback of the output voltage of the *j*th MII, respectively. i^*_{Lj} and i_{Lfj} are defined as the reference and feedback of the inductor current of the *j*th MII, respectively. $G_{dj}(\mathrm{s})$ represents the input voltage regulator with PI regulation of the *j*th MII. $G_{oj}(\mathrm{s})$ is the output voltage regulator with PR regulation of the *j*th MII. $G_{ij}(\mathrm{s})$ is defined as the inductor current regulator with PR regulation of the *j*th MII. $G_{qi}(\mathrm{s})$ represents the reactive power regulator with P regulation of the *j*th MII as well. S_j is defined as a signal in the control system of the *j*th MII.

1) Active Power Regulation: According to Fig. 4, it can be seen that each MII has its own MPPT function. The classic perturb and observe technique can be used as the MPPT algorithm. Since $\sin\theta$ is aligned with the PCC voltage in the PLL, the input voltage controller (i.e., $G_{dj}(\mathrm{s})$) can be regarded as the active power regulator. The single-stage H-bridge inverter is used as the inverter topology. Thus, the input voltage of each MII has the double-line-frequency oscillation. As a result, for the active power control loop, since the line frequency is 50 Hz, the cutoff frequency of the input voltage control loop should be designed less than 100 Hz. The amplitude of $U_{\mathrm{ord}j}$ can represent the active power of the *j*th MII. Therefore, the active power sharing between SC-MIIs is dependent on their individual maximum power available from PV panels. Therefore, since the same grid-tied current flows through ac side of each MII, the MII with larger power harvested from PV panels has higher output voltage.

2) Reactive Power Regulation: From Fig. 4, it can be seen that the instantaneous output voltage reference of each MII (i.e., u^*_{oj}) is synthesized with two components. The first component is the output of active power control loop, *i.e.*, $U_{\mathrm{ord}j}$ multiplied by the $\sin\theta$. The second component is the output of reactive power control loop, *i.e.*, $U_{\mathrm{orq}j}$ multiplied by $-\cos\theta$. The phase of this component lags the PCC voltage with 90°. The reactive power reference (i.e., $Q_{\mathrm{of}j}$) is derived as

$$Q^*_{oj} = P_{oj}\frac{\sqrt{1-\lambda^2}}{\lambda} \tag{3}$$

where λ is the value of the power factor, which is determined by the utility grid commands. P_{oj} is the average output active power of the *j*th MII, which enables its reactive power regulator.

Assuming that the *j*th MII enables its own reactive power control loop, the value of the control signal (i.e., S_j) is set to 1. Therefore, the output of the reactive power control loop is added to the instantaneous output voltage reference. The reference vector of the output voltage lags the PCC voltage vector. From Fig. 3(b), the output voltage vector of this MII lags the PCC voltage vector. While the reactive power control loops of the other MIIs are disabled, the values of the control signals are set to 0. Therefore, instantaneous reference vectors of the output voltages in these MIIs are in phase with the PCC voltage vector. From Fig. 3(b), the output voltage vectors of these MII lead the PCC voltage vector. As a result, the adjustable power factor of the grid-tied SC-MII system is realized, and there is a communication link between each MIIs.

3) Voltage and Current Regulation: From Fig. 4, it can be seen that each MII has its own output voltage regulator and inductor current regulator. The voltage and current control loops of the MII are similar to the conventional single-phase inverter. Therefore, the control bandwidth of the inductor current control

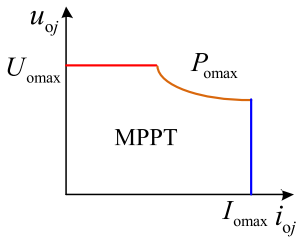

Fig. 5. Output characteristic curve of the SC-MIIs.

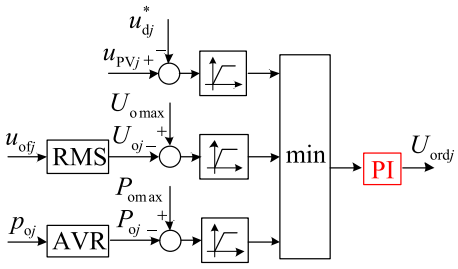

Fig. 6. Control scheme of three output limits.

loop is the highest, and the cutoff frequency is usually designed between 1/20 and 1/10 times of the switching frequency. The control bandwidth of the output voltage control loop is lower than that of the inductor current control loop, and the cutoff frequency is usually designed between 10 and 20 times of the fundamental frequency. Since the reactive power of each MII is not regulated frequently, the proportional coefficient of the reactive power regulator can be very small. The design method of the input voltage regulator is the same as the conventional PV grid-tied inverter.

B. Operation Limitations

Since the single-phase full-bridge inverter topology is used, the output voltage of each MII should be lower than its input voltage to avoid overmodulation. Therefore, if the power conditioning stage of the SC-MIIs is single stage, the output voltage of each MII should be lower than the output voltage of its interfaced PV panel. On the other hand, the output current of each MII should be limited within a suitable range, which is dependent on the current rating of the adopted power devices [14], [15], [17]. Therefore, the output characteristics of the MII are depicted in Fig. 5, where $P_{o\max}$ represents the maximum output power of each MII, and $I_{o\max}$ represents the maximum output current of each MII. $U_{o\max}$ is defined as the maximum output voltage of each MII, and the amplitude of $U_{o\max}$ is related to the PV panel voltage. $U_{o\max}$ can be written as

$$U_{o\max} = M \cdot u_{\mathrm{PV}} \tag{4}$$

where *M* is the modulation index of the MII.

The output current limitation of the *j*th MII can be achieved by limiting the maximum value of the i^*_{Lj}. The control scheme of output voltage and power limitation is shown in Fig. 6, where U_{oj} is the root-mean-square (RMS) value of the $u_{\mathrm{of}j}$. P_{oj} represents the average value of the instantaneous power p_{oj}.

From Fig. 6, it can be seen that, when the output voltage and the output power of the *j*th MII are less than their maximum limitations, the input voltage control loop is enabled. Extracting the maximum available power from the *j*th PV panel can be achieved in mismatched conditions. However, when the output voltage or the output power of the *j*th MII is limited by the maximum constraint, $u_{\mathrm{PV}j}$ will be higher than u^*_{dj}. As a result, extracting the maximum available power from the *j*th PV panel cannot be achieved. Therefore, the limited voltage and current ratings of the adopted power devices are the main drawbacks not only for the SC-MIIs structure, but also for other structures with series-connected converters.

C. Simulation Results

The grid-tied SC-MII PV generation system with the proposed control strategy is conducted in PSIM simulation platform. The test system with three MIIs is taken as an example. The PV panels are emulated by using dc power supplies series connected with resistors. The input voltage of each MII is controlled as 36 V. The series resistance in the dc source is adjusted to emulate the variable PV power, so the input power mismatch of each MII was thereby achieved.

1) Unity Power Factor: Fig. 7 shows the steady-state and dynamic waveforms of three MIIs with unity power factors, where u_{grid} and i_{o} represent the utility grid voltage and the grid-tied current, respectively. u_{o1} to u_{o3} are defined as the output voltages of three MIIs. $u_{\mathrm{PV}1}$ to $u_{\mathrm{PV}3}$ represent the output voltages of three PV panels. P_{o1} to P_{o3} are defined as the output power of three MIIs feeding into the grid, respectively.

In Fig. 7(a), the grid-tied power of MII #1 is 190 W, the grid-tied power of MII #2 is 230 W, and the grid-tied power of MII #3 is 130 W. Therefore, the output voltage of MII #2 is the highest, and the output voltage of MII #3 is the lowest. The grid-tied current is in phase with the utility grid voltage. In Fig. 7(b), the grid-tied power of MII #3 increases at 0.8 s. After 0.8 s, the grid-tied power of MII #3 is the largest, and the output voltage of MII #3 is the highest.

2) Nonunity Power Factor: Fig. 8 shows the steady-state waveforms of three MIIs with nonunity power factors, where u^*_{o1} to u^*_{o3} are defined as the output voltage references of three MIIs. i^*_{L1} to i^*_{L3} are defined as the voltage regulator outputs of three MIIs. The line impedance is set to zero in simulations; thus, the utility grid voltage can be regarded as the PCC voltage.

As shown in Fig. 8(a), the grid-tied power of MII #1 is 190 W, the grid-tied power of MII #2 is 240 W, and the grid-tied power of MII #3 is 130 W. The power factor is set to 0.92 (lagging), and the reactive power regulator in MII #1 is enabled. Therefore, the output voltage of MII #2 is the highest, and the output voltage of MII #3 is the lowest. The phase angle of grid-tied current lags the utility grid voltage. As shown in Fig. 8(b) and the zoom-in results of the zero-crossing parts, it can be seen that the output voltages of MII #2 and MII #3 lead the PCC voltage, while the output voltage of MII #1 lags the PCC voltage. Moreover, the output voltage references of MII #2 and MII #3 are in phase

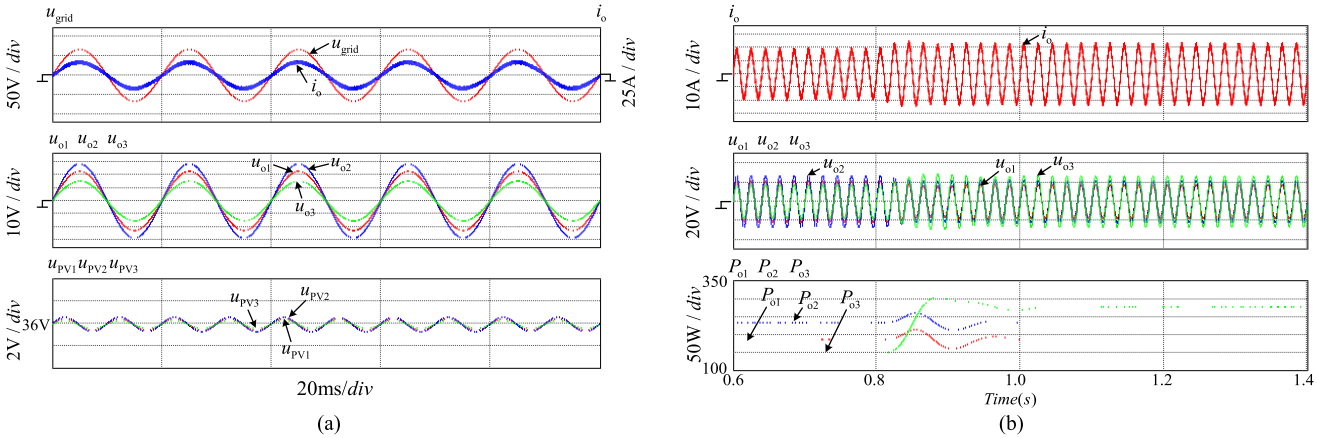

Fig. 7. Simulation results with unity power factor. (a) Steady-state waveforms with different output power. (b) Dynamic waveforms.

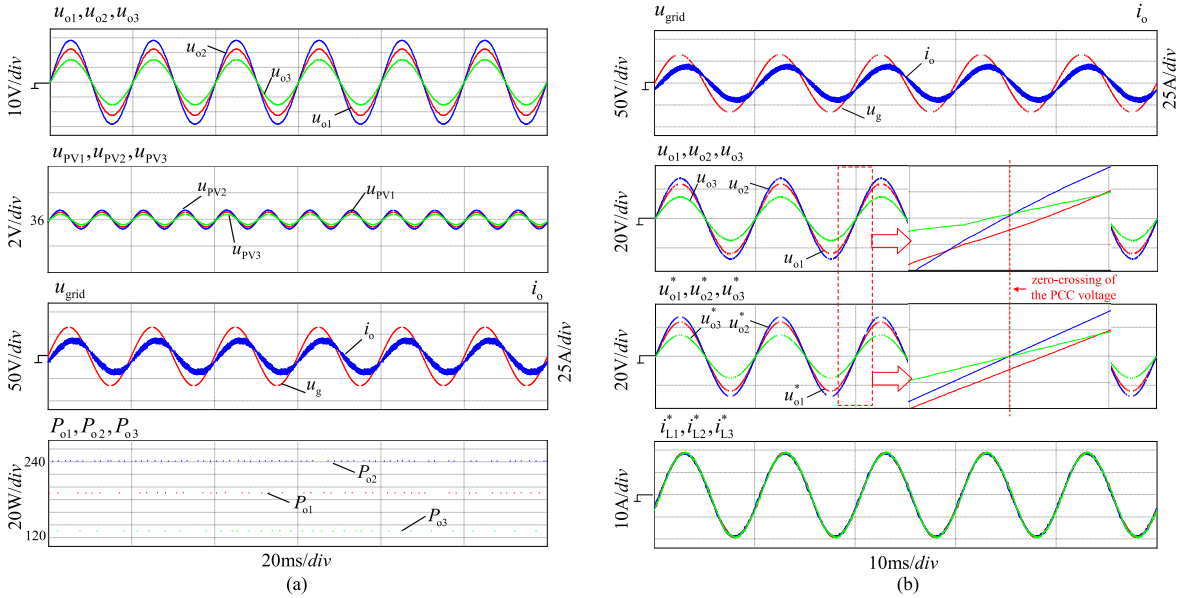

Fig. 8. Steady-state simulation results with nonunity power factor. (a) Output power of three MIIs. (b) Output voltages of three MIIs.

with the PCC voltage, while the output voltage reference of MII #1 lags the PCC voltage.

Fig. 9 shows the dynamic waveforms of three MIIs with nonunity power factors. In Fig. 9, the power factor of the grid-tied SC-MII system is set from 0.92 (leading) to 0.92 (lagging). It can be seen that the performance of reactive power regulation is as expected. The output voltages of three MIIs are stable. On the other hand, it is worth mentioning that if MII #1 is under fault condition, the grid-tied SC-MII system is still stable. Since the active power control of each MII is distributed and dependent on the individual maximum power available from PV panels, the rest of the MIIs are operating with unity power factor until another MII is selected to enable its reactive power regulator.

IV. Experimental Results

In order to verify the grid-tied SC-MII PV generation system and its corresponding control, a downscaled PV system prototype including three single-stage MIIs has been built in the laboratory. The picture of the grid-tied SC-MII system is shown in Fig. 10.

The PV panels were emulated by using dc power supplies series with resistors in the experiments, and the input voltage of each MII is controlled as 36 V. The PV power mismatch is achieved by changing the series resistance of each dc power supply. The utility grid was emulated by an ac voltage source, and the voltage was set to 46 V. The control circuit of each MII was implemented based on DSP TMS320F2808. The specifications of each MII are listed in Table I. The value of filter inductors (shown in Fig. 2) is 130 μH. The reactive power regulator of MII #1 is enabled, and the reactive power command is transferred by CAN2.0 communication.

The experimental results of the grid-tied SC-MII system with unity power factor are shown in Fig. 11, where u_{o1}, u_{o2}, and u_{o3} represent the output voltages of three MIIs, respectively. i_o represents the grid-tied current.

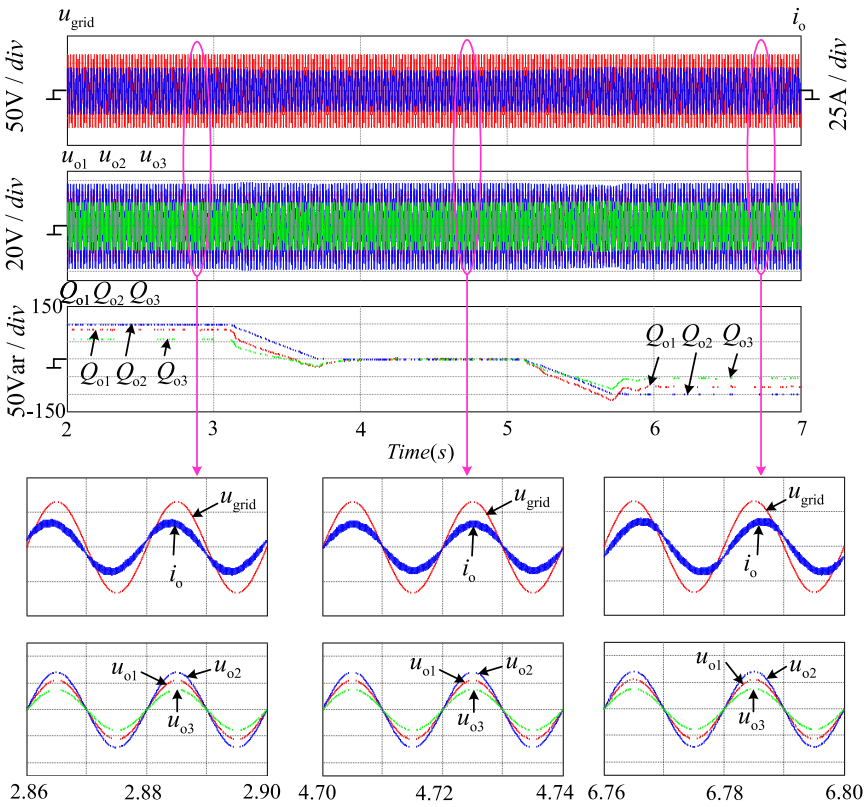

Fig. 9. Dynamic simulation results with nonunity power factor.

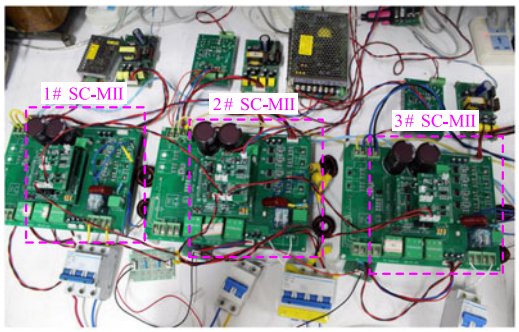

Fig. 10. Picture of the grid-tied SC-MII system.

TABLE I
PARAMETERS OF EACH SC-MII

Parameter	Value
Input voltage	0–45 V
Output voltage	0–30 V
Grid-tied current	0–10 A
Rated power	250 W
Switching frequency	100 kHz
Grid voltage	46 V
Grid frequency	50 Hz
Filter inductor (L_1 and L_2)	130 μH
Filter capacitor (C_o)	25 μF
DC input filter capacitor	1000 μF
MOSFET	IRFP3415PBF (150 V)

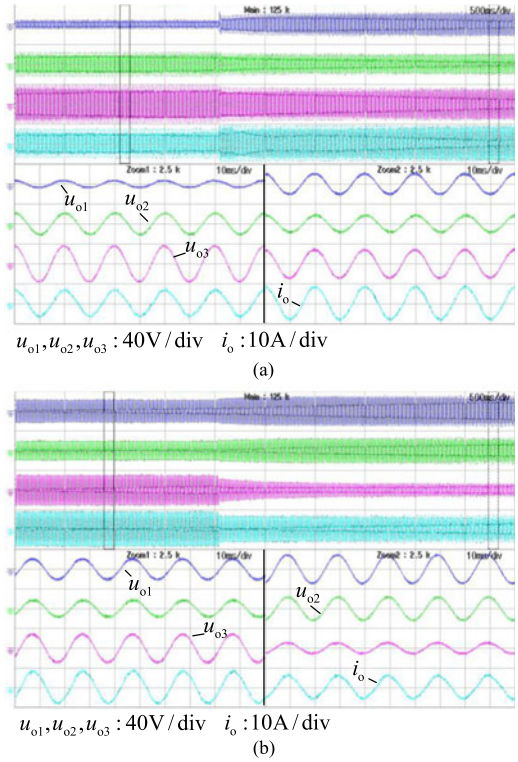

Fig. 11. Dynamic waveforms with unity power factor. (a) $P_{o1} = P_{o2} = P_{o3} = 125$ W. (b) $P_{o1} = 83$ W, $P_{o2} = 125$ W, and $P_{o3} = 167$ W.

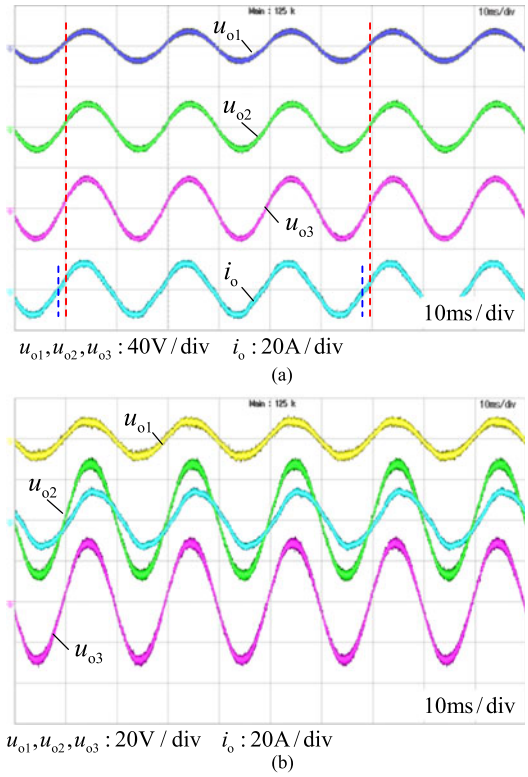

Fig. 12. Steady-state waveforms with nonunity power factor. (a) $P_{o1} = 83\,\text{W}$, $P_{o2} = 125\,\text{W}$, $P_{o3} = 167\,\text{W}$, and $Q_S = -100\,\text{Var}$. (b) $P_{o1} = 65\,\text{W}$, $P_{o2} = 180\,\text{W}$, $P_{o3} = 195\,\text{W}$, and $Q_S = 100\,\text{Var}$.

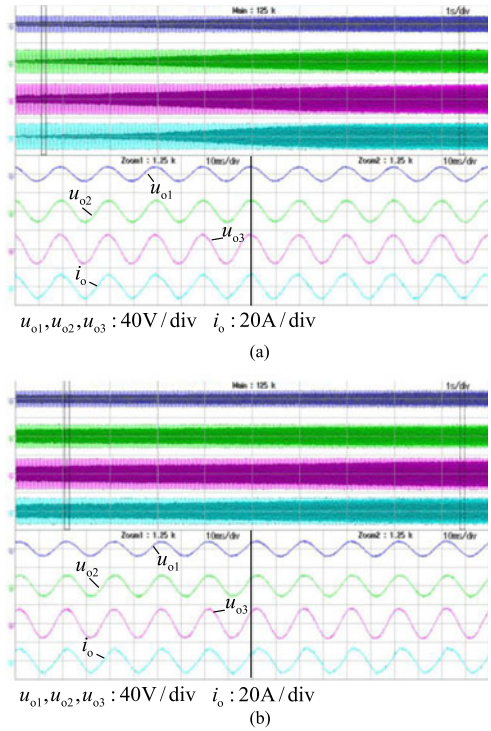

Fig. 13. Dynamic waveforms with nonunity power factor. (a) Q_S is from 0 to –100 Var, $P_{o1} = 83\,\text{W}$, $P_{o2} = 125\,\text{W}$, and $P_{o3} = 167\,\text{W}$. (b) Q_S is from 0 to –100 Var, $P_{o1} = 83\,\text{W}$, $P_{o2} = 125\,\text{W}$, and $P_{o3} = 167\,\text{W}$.

In Fig. 11(a), it is shown that $P_{o1} = 65\,\text{W}$, $P_{o3} = 110\,\text{W}$, and P_{o1} is changed from 20 W to 80 W. The reactive power is set to zero. It can be seen that, when P_{o1} increases, the output voltage of MII #1 increases as well. Since the total voltage of three MIIs is clamped by the ac voltage source, both the output voltages of MII #2 and MII #3 decrease. The grid-tied current increases and it is still in phase with the utility grid voltage. In Fig. 11(b), it is shown that $P_{o1} = 80\,\text{W}$, $P_{o2} = 65\,\text{W}$, and P_{o3} is changed from 110 to 30 W. It can be seen that, when P_{o3} decreases, the output voltage of MII #3 decreases as well. Since the total voltage of three MIIs is clamped by the ac voltage source, the output voltages of MII #1 and MII #2 increase. It is indicated that the output voltage of each MII is dependent on the power available from its interfaced PV panel, and the grid-tied SC-MII system has great dynamic performance with a transient output voltage regulation process.

The experimental results of the grid-tied SC-MII system with nonunity power factor are shown in Figs. 12 and 13. Q_S represents the total reactive power of the grid-tied SC-MII system.

In Fig. 12(a), it is shown that $P_{o1} = 83\,\text{W}$, $P_{o2} = 125\,\text{W}$, $P_{o3} = 167\,\text{W}$, and the reactive power is set to –100 Var. As a result, it can be seen that the output voltage of MII #3 is the highest, which equals to 19.6 V. The output voltage of MII #2 is 14.7 V, and the output voltage of MII #1 is the lowest. The grid-tied current leads the utility grid voltage. In Fig. 12(b), $P_{o1} = 65\,\text{W}$, $P_{o2} = 180\,\text{W}$, $P_{o3} = 195\,\text{W}$, and the reactive power is set to 100 Var. It can be seen that the grid-tied current lags the utility grid voltage. According to Fig. 12, it is indicated that the output voltage of each MII is only dependent on the power available from its interfaced PV panel. One of the MIIs has the ability to regulate the total reactive power of the grid-tied SC-MII system.

In Fig. 13(a), it is shown that $P_{o1} = 83\,\text{W}$, $P_{o2} = 125\,\text{W}$, $P_{o3} = 167\,\text{W}$, and the reactive power is changed from 0 to –100 Var. It can be seen that, when the reactive power is changed, the voltages of three MIIs are stable, but the grid-tied current leads the utility grid voltage. In Fig. 13(b), it is shown that $P_{o1} = 83\,\text{W}$, $P_{o2} = 125\,\text{W}$, $P_{o3} = 167\,\text{W}$, and the reactive power is changed from 0 to 100 Var. It can be seen that, when the reactive power is changed, the voltages of three MIIs are stable, but the grid-tied current lags the utility grid voltage. As a result, it is indicated that the dynamic process of reactive power variation is smooth, and the dynamic performance of the grid-tied SC-MII system is good.

V. Conclusion

A distributed control strategy for the grid-tied SC-MII PV generation system is proposed in this paper, and both the active and reactive power control of each MII are analyzed and presented. Simulation and experimental results demonstrate the following:

1) The output voltage of each MII is at ac line frequency, and the active power sharing among the MIIs is dependent on the individual maximum power available from PV panels. Therefore, the distributed active power control of each MII is achieved.

2) The output voltage of each MII is almost in phase with the utility grid with either unity or nonunity power factor. Furthermore, the proposed distributed control has the ability to regulate the reactive power and to provide reactive power support for the utility grid.

Hence, both the grid-tied SC-MII system and the proposed distributed control is a good potential solution for distributed and grid-tied PV generation systems.

REFERENCES

[1] J. Chavarria, D. Biel, F. Guinjoan, C. Meza, and J. J. Negroni, "Energy-balance control of PV cascaded multilevel grid-connected inverters under level-shifted and phase-shifted PWMs," *IEEE Trans. Ind. Electron.*, vol. 60, no. 1, pp. 98–111, Jan. 2013.

[2] S. B. Kjaer, J. K. Pederson, and F. Blaabjerg, "A review of single-phase grid-connected inverters for photovoltaic modules," *IEEE Trans. Ind. Appl.*, vol. 41, no. 5, pp. 1292–1306, Sep./Oct. 2005.

[3] P. Mazumdar, P. N. Enjeti, and R. S. Balog, "Analysis and design of smart PV modules," *IEEE J. Emerg. Sel. Topics Power Electron.*, vol. 2, no. 3, pp. 451–459, Sep. 2013.

[4] X. Guo, "Three-phase CH7 inverter with a new space vector modulation to reduce leakage current for transformerless photovoltaic systems," *IEEE J. Emerg. Sel. Topics Power Electron.*, vol. 2, no. 5, pp. 708–712, Jun. 2017.

[5] E. Villanueva, P. Correa, J. Rodriguez, and M. Pacas, "Control of a single-phase cascaded H-bridge multilevel inverter for grid-connected photovoltaic systems," *IEEE Trans. Ind. Electron.*, vol. 56, no. 11, pp. 4399–4406, Nov. 2009.

[6] C. Olalla, D. Clement, M. Rodriguez, and D. Maksimovic, "Architectures and control of submodule integrated dc-dc converters for photovoltaic applications," *IEEE Trans. Power Electron.*, vol. 28, no. 6, pp. 2980–2997, Jun. 2013.

[7] Q. Li and P. Wolfs, "A review of the single phase photovoltaic module integrated converter topologies with three different dc link configuration," *IEEE Trans. Power Electron.*, vol. 23, no. 3, pp. 1320–1333, May 2008.

[8] A. Bidram, A. Davoudi, and R. S. Balog, "Control and circuit techniques to mitigate partial shading effects in photovoltaic arrays," *IEEE J. Photovoltaics*, vol. 2, no. 4, pp. 532–546, Oct. 2012.

[9] H. Hu *et al.*, "A three-port flyback for PV microinverter applications with power pulsation decoupling capability," *IEEE Trans. Power Electron.*, vol. 27, no. 9, pp. 3953–3964, Sep. 2012.

[10] Z. Zhang, X. He, and Y. Liu, "An optimal control method for photovoltaic grid-tied-interleaved flyback microinverters to achieve high efficiency in wide load range," *IEEE Trans. Power Electron.*, vol. 28, no. 11, pp. 5074–5087, Nov. 2013.

[11] A. Nanakos, E. Tatakis, and N. Papanikolaou, "A weighted-efficiency-oriented design methodology of flyback inverter for ac photovoltaic," *IEEE Trans. Power Electron.*, vol. 27, no. 7, pp. 3221–3233, Jul. 2012.

[12] A. I. Bratcu, I. Munteanu, S. Bacha, D. Picault, and B. Raison, "Cascaded dc-dc converter photovoltaic systems: power optimization issues," *IEEE Trans. Ind. Electron.*, vol. 58, no. 2, pp. 403–411, Feb. 2011.

[13] N. Femia, G. Lisi, G. Petrone, G. Spagnuolo, and M. vitelli, "Distributed maximum power point tracking of photovoltaic arrays: Novel approach and system analysis," *IEEE Trans. Ind. Electron.*, vol. 55, no. 7, pp. 2610–2621, Jul. 2008.

[14] M. Balato, M. Vitelli, N. Femia, G. Petrone, and G. Spagnuolo, "Factors limiting the efficiency of DMPPT in PV applications," in *Proc. IEEE 3rd Int. Conf. Clean Electr. Power*, Ischia, Italy, Jun. 14–16, 2011, pp. 604–608.

[15] R. Alonso, E. Roman, A. Sanz, V. E. M. Santos, and P. Ibanez, "Analysis of inverter-voltage influence on distributed MPPT architecture performance," *IEEE Trans. Ind. Electron.*, vol. 59, no. 10, pp. 3900–3907, Oct. 2012.

[16] M. Vitelli, "On the necessity of joint adoption of both distributed maximum power point tracking and central maximum power point tracking in PV systems," *Prog. Photovoltaic, Res. Appl.*, vol. 22, no. 3, pp. 283–299, Mar. 2014.

[17] M. Balato and M. Vitelli, "A new control strategy for the optimization of distributed MPPT in PV applications," *Int. J. Electr. Power Energy Syst.*, vol. 62, pp. 763–773, Nov. 2014.

[18] M. Balato and M. Vitelli, "An algorithm for the fast estimate of the maximum power voltages in PV applications adopting microconverters," *COMPEL Int. J. Comput. Math Electr. Electron. Eng.*, vol. 34, no. 1, pp. 110–131, Jan. 2015.

[19] P. S. Shenoy, K. A. Kim, B. B. Johnson, and P. T. Krein, "Differential power processing for increased energy production and reliability of photovoltaic systems," *IEEE Trans. Power Electron.*, vol. 28, no. 6, pp. 2968–2979, Jun. 2013.

[20] K. A. Kim, P. S. Shenoy, and P. T. Krein, "Converter rating analysis for photovoltaic differential power processing systems," *IEEE Trans. Power Electron.*, vol. 28, no. 6, pp. 2968–2979, Jun. 2013.

[21] L. F. L. Villa, T.-P. Ho, J.-C. Crebier, and B. Raison, "A power electronics equalizer application for partially shaded photovoltaic modules," *IEEE Trans. Ind. Electron.*, vol. 60, no. 3, pp. 1179–1190, Mar. 2013.

[22] M. Abolhassani, "Modular multipulse rectifier transformers in symmetrical cascaded H-bridge medium voltage drive," *IEEE Trans. Power Electron.*, vol. 30, no. 4, pp. 1987–1997, Apr. 2015.

[23] K. Sano and M. Takasaki, "A transformerless D-STATCOM based on a multi-voltage cascaded converter requiring no dc source," *IEEE Trans. Power Electron.*, vol. 27, no. 6, pp. 2783–2795, Jun. 2012.

[24] C. D. Townsend, T. J. Summers, J. Vodden, A. J. Watson, R. E. Betz, and J. C. Clare, "Optimization of switching losses and capacitor voltage ripple using model predictive control of a cascaded H-bridge multilevel StatCom," *IEEE Trans. Power Electron.*, vol. 28, no. 7, pp. 3077–3087, Jul. 2013.

[25] T. Zhao, G. Wang, S. Battacharya, and A. Q. Huang, "Voltage and power balance control for cascaded H-bridge converter-based solid-state transformer," *IEEE Trans. Power Electron.*, vol. 28, no. 4, pp. 1523–1532, Apr. 2013.

[26] L. Liu, H. Li, and Y. Xue, "A coordinated active and reactive power control strategy for grid-connected cascaded photovoltaic (PV) system in high voltage high power applications," in *Proc. IEEE 28th Appl. Power Electron. Conf. Expo.*, Long Beach, CA, USA, Mar. 17–21, 2013, pp. 1301–1308.

[27] Y. Zhou, L. Liu, and H. Li, "A high-performance photovoltaic module-integrated converter (MIC) based on cascaded quasi-z-source inverters (qZSI) using eGaN FETs," *IEEE Trans. Power Electron.*, vol. 28, no. 6, pp. 2727–2738, Jun. 2013.

[28] L. Liu, H. Li, Y. Xue, and W. Liu, "Reactive power compensation and optimization strategy for grid-interactive cascaded photovoltaic systems," *IEEE Trans. Power Electron.*, vol. 30, no. 1, pp. 188–202, Jan. 2015.

[29] Y. Zhou and H. Li, "Analysis and suppression of leakage current in cascaded-multilevel-inverter-based PV systems," *IEEE Trans. Power Electron.*, vol. 29, no. 10, pp. 5265–5277, Oct. 2014.

[30] L. Liu, H. Li, Y. Xue, and W. Liu, "Decoupled active and reactive power control for large-scale grid-connected photovoltaic systems using cascaded modular multilevel converters," *IEEE Trans. Power Electron.*, vol. 0, no. 1, pp. 176–187, Jan. 2015.

[31] M. Nuotio, M. Ilic, Y. Liu, J. Bonanno, and P. J. Verlinden, "Innovative AC photovoltaic module system using series connection and universal low-voltage micro inverters," in *Proc. 40th IEEE Photovoltaic Spec. Conf.*, Denver, CO, USA, Oct. 15, 2014, pp. 1367–1369.

[32] F. Lu, B. Choi, and D. Maksimovic, "Autonomous control of series-connected low voltage photovoltaic microinverters," in *Proc. 16th IEEE Workshop Control Model. Power Electron.*, Vancouver, BC, Canada, Jul. 12–15, 2015, pp. 1–6.

Li Zhang (S'11–M'13) received the B.S. and Ph.D. degrees in electrical engineering from Nanjing University of Aeronautics and Astronautics, Nanjing, China, in 2007, and 2012, respectively.

In 2014, he joined the Faculty of Electrical Engineering, Hohai University, Nanjing, China, where he is currently an Associate Professor. From October 2012 to September 2014, he was a Postdoctoral Research Fellow with the Department of Electrical Engineering, Tsinghua University, Beijing, China. From July to August 2014, he was a Visiting Scholar with the Department of Energy Technology, Aalborg University, Denmark. From October 2016 to October 2017, he was a Visiting Scholar with the Department of Electrical and Computer Engineering, Ryerson University, Canada. His current research interests include topology, control of dc–ac converters, and distributed generation technology.

Dr. Zhang was a recipient of the IEEE TRANSACTIONS ON POWER ELECTRONICS Outstanding Reviewer Award in 2014.

Kai Sun (M'12–SM'16) received the B.E., M.E., and Ph.D. degrees in electrical engineering from Tsinghua University, Beijing, China, in 2000, 2002, and 2006, respectively.

In 2006, he joined the Faculty of Electrical Engineering, Tsinghua University, where he is currently an Associate Professor. From September 2009 to August 2010, he was a Visiting Scholar with the Department of Energy Technology, Aalborg University, Aalborg, Denmark. From January to August 2017, he was a Visiting Professor with the Department of Electrical and Computer Engineering, University of Alberta, Edmonton, AB, Canada. His current research interests include power electronics for renewable generation systems, microgrids, and active distribution networks.

Dr. Sun is a member of the IEEE Power Electronics Society Sustainable Energy Systems Technical Committee, the IEEE Power Electronics Society Power and Control Core Technologies Committee, and the IEEE Industrial Electronics Society Renewable Energy Systems Technical Committee, and the IEEE IAS Industrial Drive Committee Awards Subcommittee. He is an Associate Editor for the IEEE TRANSACTIONS ON POWER ELECTRONICS, the IEEE JOURNAL OF EMERGING AND SELECTED TOPICS IN POWER ELECTRONICS, and the *Journal of Power Electronics*. He served as the TPC Vice Chair of the 2017 IEEE Energy Conversion Congress and Exposition (ECCE) and the IEEE ECCE-Asia2017. He was a recipient of the Delta Young Scholar Award in 2013 and the Youth Award of China Power Supply Society in 2017.

Yun Wei Li (S'04–M'05–SM'11) received the B.Sc. degree in engineering degree in electrical engineering from Tianjin University, Tianjin, China, in 2002, and the Ph.D. degree from Nanyang Technological University, Singapore, in 2006.

In 2005, he was a Visiting Scholar with Aalborg University, Denmark. From 2006 to 2007, he was a Postdoctoral Research Fellow with Ryerson University, Canada. In 2007, he also worked at Rockwell Automation Canada before he joined University of Alberta, Edmonton, AB, Canada, in the same year. Since then, he has been with the University of Alberta, where he is currently a Professor. His research interests include distributed generation, microgrids, renewable energy, high-power converters, and electric motor drives.

Dr. Li is an Associate Editor for the IEEE TRANSACTIONS ON POWER ELECTRONICS, the IEEE TRANSACTIONS ON INDUSTRIAL ELECTRONICS, the IEEE TRANSACTIONS ON SMART GRID, and the IEEE JOURNAL OF EMERGING AND SELECTED TOPICS IN POWER ELECTRONICS. He received the Richard M. Bass Outstanding Young Power Electronics Engineer Award from the IEEE Power Electronics Society in 2013 and the Second Prize Paper Award of the IEEE TRANSACTIONS ON POWER ELECTRONICS in 2014.

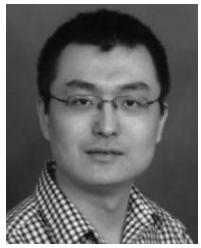

Xiaonan Lu (S'12–M'13) received the B.E. and Ph.D. degrees in electrical engineering from Tsinghua University, Beijing, China, in 2008 and 2013, respectively.

From September 2010 to August 2011, he was a guest Ph.D. student with the Department of Energy Technology, Aalborg University, Aalborg, Denmark. From October 2013 to December 2014, he was a Postdoctoral Researcher with the Department of Electrical Engineering and Computer Science, University of Tennessee, Knoxville. In January 2015, he joined the Energy Systems Division, Argonne National Laboratory, Lemont, IL, USA. He also holds an adjunct position at the Northwestern-Argonne Institute of Science and Engineering, Northwestern University. His research interests include modeling and control of power electronic converters in ac and dc microgrids, hardware-in-the-loop real-time simulation, and distribution automation.

Dr. Lu received the Outstanding Reviewer Award for the IEEE TRANSACTIONS ON POWER ELECTRONICS in 2013, the Outstanding Reviewer Award for the IEEE TRANSACTIONS ON SMART GRID in 2015, and the Outstanding Postdoctoral Performance Award in Argonne National Laboratory in 2016. He is an Editor for the IEEE TRANSACTIONS ON SMART GRID, an Associate Editor for the IEEE TRANSACTIONS ON INDUSTRY APPLICATIONS, and a Guest Associate Editor of the Special Issues entitled "Structured DC Microgrids" and "Asynchronous Interconnect and Generation" in the IEEE JOURNAL OF EMERGING AND SELECTED TOPICS OF POWER ELECTRONICS. He is a member of the IEEE Power Electronics Society, the IEEE Industry Applications Society (IAS), the IEEE Power and Energy Society, and the IEEE Industrial Electronics Society. He was also elected as the Secretary of Industrial Power Converter Committee in the IEEE IAS.

Jinquan Zhao (M'06) received the B.S. and Ph.D. degrees in electrical engineering from Shanghai Jiao Tong University, Shanghai, China, in 1993 and 2000, respectively.

He was a Postdoctoral Associate with Cornell University, Ithaca, NY, USA, from 2000 to 2003, and Tsinghua University, Beijing, China, from 2004 to 2005. In 2006, he joined the Faculty of Electrical Engineering, Hohai University, Nanjing, China, where he is currently a Professor. His current research interests include voltage stability analysis and control, optimal power flow, and its applications.